Published in final edited form as:
Matrix Biol. 2010 May ; 29(4): 304–316. doi:10.1016/j.matbio.2010.01.005.

Reduced versican cleavage due to *Adamts9* haploinsufficiency is associated with cardiac and aortic anomalies

Christine B. Kern, Ph.D[a,*], **Andy Wessels, Ph.D.**[a], **Jessica McGarity**[a], **Laura J. Dixon**[b], **Ebony Alston**[a], **W. Scott Argraves, Ph.D.**[a], **Danielle Geeting**[a], **Courtney M. Nelson**[b], **Donald R. Menick, Ph.D**[c], and **Suneel S. Ape, M.B.B.S., D.Phil**[b]

[a]Department of Regenerative Medicine and Cell Biology, 171 Ashley Avenue, Medical University of South Carolina, Charleston, SC 29425, USA

[b]Department of Biomedical Engineering, Lerner Research Institute ND-20, Cleveland Clinic, 9500 Euclid Avenue, Cleveland OH 44195, USA

[c]Department of Medicine Division of Cardiology, Room 201 114 Doughty Street, Medical University of South Carolina, Charleston, SC 29425

Abstract

Here, we demonstrate that ADAMTS9, a highly conserved versican-degrading protease, is required for correct cardiovascular development and adult homeostasis. Analysis of *Adamts9*$^{+/LacZ}$ heterozygous adult mice revealed anomalies in the aortic wall, valvulosinus and valve leaflets. Abnormal myocardial projections and `spongy' myocardium consistent with non-compaction of the left ventricle were also found in *Adamts9*$^{+/LacZ}$ mice. During development, *Adamts9* was expressed in derivatives of the Secondary Heart Field, vascular smooth muscle cells (VSMC) in the arterial wall, mesenchymal cells of the valves, and non-myocardial cells of the ventricular myocardium but expression also continued in the adult heart and ascending aorta. Thus, the adult cardiovascular anomalies found in *Adamts9*$^{+/LacZ}$ hearts could result from subtle developmental alterations in extracellular matrix remodeling or defects in adult homeostasis. The valvular and aortic anomalies of *Adamts9*$^{+/LacZ}$ hearts were associated with accumulation of versican and a decrease in cleaved versican relative to WT littermates. These data suggest a potentially important role for ADAMTS9 cleavage of versican, or other, as yet undefined substrates in development and allostasis of cardiovascular extracellular matrix. In addition these studies identify *ADAMTS9* as a potential candidate gene for congenital cardiac anomalies. Mouse models of ADAMTS9 deficiency may be useful to study myxomatous valve degeneration.

*denotes corresponding author Dr. Christine B. Kern 173 Ashley Avenue Charleston SC, 29525-0025 kernc@musc.edu FAX: 843 792-0664 Phone: 843 792-9618.
Dr. Andy Wessels: wesselsa@musc.edu
Ms. Jessica McGarity: mcgarityjd@gmail.com
Ms. Laura Dixon: collin3@ccf.org
Ms. Ebony Alston: alstone@musc.edu
Dr. W. Scott Argraves: argraves@musc.edu
Ms. Danielle Geeting: dngeeting@gmail.com
Ms. Courtney Nelson: nelsonc5@ccf.org
Dr. Donald Menick: menickd@musc.edu
Dr. Suneel S. Apte: APTES@ccf.org

Disclosures: None to disclose from any author.

Keywords

ADAMTS; versican; extracellular matrix; myxomatous valves

1. Introduction

Congenital heart disorders are relatively common in children, and can lead to high morbidity and mortality. Cardiovascular conditions that first become apparent in the adult may well be rooted in subtle developmental defects that remain latent until uncovered by cumulative hemodynamic stresses in adulthood. The cardiac and vascular extracellular matrix (ECM) has a critical mechanical role, and is likely to have a key role in signaling and morphogenesis. Therefore, defects in ECM or ECM modifying enzymes could be among the many causes of inherited and adult-onset cardiovascular disorders. The ECM of the primary mouse heart tube is of an immature, transitional type, i.e. rich in hyaluronan, versican and fibronectin, to facilitate cell migration, growth, and dynamic morphological changes that give rise to the four-chambered heart. As development progresses, this transitional ECM is remodeled to form the highly specialized connective tissue of the adult heart. The mature cardiovascular ECM is a composite of collagens, proteoglycans, and elastin that is highly organized in response to specific regional mechanical demands, and it can be remodeled in an adaptive response to an altered mechanical environment.

The cardiac outlet, valves and septal structures of the heart originate from endocardial cushions that are comprised of ECM rich in the proteoglycan versican, fibulin-1, fibronectin, cartilage link protein and hyaluronan (Cooley et al., 2008; Kern et al., 2007; Wirrig et al., 2007). Versican forms large water-retaining aggregates with hyaluronan that are stabilized by link protein, and these aggregates constitutes an important volume occupying entity in the matrix. Versican and hyaluronan have been shown to be essential for the subjacent endocardium to undergo an epithelial to mesenchymal transition (EMT) for the production of cardiac mesenchyme (Camenisch et al., 2001; Camenisch et al., 2002; Mjaatvedt et al., 2001). The ECM of the cardiac outlet in the primary heart guides the migration of extra cardiac cells originating from the Secondary Heart Field (SHF) (Kelly et al., 2001; Mjaatvedt et al., 2001), and cardiac neural crest (CNC) (Hutson and Kirby, 2007; Kirby et al., 1983; Miyagawa-Tomita et al., 1991; Nakamura et al., 2006; Poelmann et al., 1998; Verberne et al., 1998).

Versican is a large secreted chondroitin sulfate proteoglycan that is important for cardiac development, and is also implicated in adult cardiovascular disease (Wight, 2005; Wight, 2008). Four splice variants of versican (V0, V1, V2, V3) have been identified, each containing two invariant domains, an N-terminal G1 domain that interacts with hyaluronan, and a C-terminal G3 domain that interacts with other ECM molecules (Aspberg et al., 1999; Margolis and Margolis, 1994; Wu et al., 2005). The variants differ in the presence (V0, V1, V2) or absence (V3) of internal glycosaminoglycan (GAGα or GAGβ) attachment domains, which are susceptible to proteolytic cleavage by ADAMTS proteases (Gao et al., 2002; Perides et al., 1995; Russell et al., 2003; Sandy et al., 2001; Somerville et al., 2003; Wu et al., 2005). Mice homozygous for a *LacZ* insertion into the versican gene (*Vcan*) are effectively null for all variants and die of cardiac defects at E10. Since V3 is primarily found in neural tissues and mice with deficiency of the V0 and V2 isoforms, survive (Dours-Zimmermann et al., 2009) the V1 isoform appears to be critical for cardiac development. Indeed, versican V1 is highly expressed in the cardiovascular system, and has been implicated in extracardiac cell guidance and migration (Capehart et al., 1999; Cooley et al., 2008; Kern et al., 2007; Mjaatvedt et al., 2001; Zanin et al., 1999). However, the role of versican, its variants, and proteolytic cleavage fragments in cardiac development and disease has not been completely elucidated.

During cardiac development versican is expressed in the early valvuloseptal structures and the "jelly-like" ECM which influences the growing ventricular myocardial cells (Henderson and Copp, 1998; Ito et al., 1995; Kern et al., 2007; Mjaatvedt et al., 1998; Shinomura et al., 1995; Zako et al., 1995), but its expression decreases substantially as development progresses (Kern et al., 2007; Kern et al., 2006). The longevity of secreted versican in ECM is regulated by proteolysis, which may allow for deposition of specialized ECM molecules such as elastin and collagen as development progresses. Recent studies have demonstrated that versican cleavage occurs throughout cardiac development (Kern et al., 2006), during atrioventricular remodeling, during key steps of cardiac outlet formation (Kern et al., 2007; Kern et al., 2006) and in the growth and compaction of the trabeculae in the ventricular myocardium (Cooley et al., 2008; Stankunas et al., 2008). Versican variants V1 and V0 are cleaved at the Glu^{441}-Ala^{442} peptide bond (V1 sequence enumeration) by proteases of the ADAMTS (A Disintegrin-like and Metalloprotease domain with ThromboSpondin type 1 motifs) family (Apte, 2009). Using an antibody that recognizes the neo-epitope released after ADAMTS cleavage of versican, it has been shown that versican cleavage products as well as ADAMTS1 are present in the mature arterial wall and are associated with arterial smooth muscle cell (SMC) migration *in vitro* (Jonsson-Rylander et al., 2005; Sandy et al., 2001; Wight, 2005). *In vivo* functional studies using adenoviral over-expression of a construct that approximates proteolytically cleaved versican, i.e., the N-terminal G1 domain, demonstrated that this fragment affected myocardial cell-cell interactions differently from the V3 isoform (Kern et al., 2007). Several studies have indicted that isolated subdomains of versican can profoundly influence cell behavior (LaPierre et al., 2007; Sheng et al., 2005; Wu et al., 2004; Yang et al., 2003; Zhang et al., 1999; Zheng et al., 2006). Therefore cleavage of versican V1 may not only alter the function of intact versican, but may uncover cryptic activities of cleaved fragments (Kern et al., 2007; Kern et al., 2006; Longpre et al., 2009; Wight, 2005). Indeed, such as effect was recently demonstrated in the developmental regulation of apoptosis during mammalian interdigital web regression (McCulloch et al).

A group of seven mammalian ADAMTS proteases (ADAMTS1, ADAMTS4, ADAMTS5, ADAMTS8, ADAMTS9, ADAMTS15, ADAMTS20) are referred to as "proteoglycanases". With the exception of ADAMTS8 and ADAMTS15, they all have been shown to cleave versican *in vitro* (Apte, 2004; Koo et al., 2006; Koo et al., 2007) and ADAMTS20 was found to be necessary for versican processing in skin *in vivo* (Silver et al., 2008). ADAMTS9 and ADAMTS20 are evolutionarily conserved and orthologs of GON-1 in *C. elegans.* During development, *Adamts9* is expressed in the primary heart tube and the mesoderm of the branchial arches, the point of origin for migration of extra cardiac cells from the secondary heart field (Jungers et al., 2005). *Adamts9* is expressed along pathways of NCC migration and in regions of NCC colonization (Jungers et al., 2005). Its evolutionary conservation, strong expression during cardiac development and ability to process versican (Somerville et al., 2003), (Jungers et al., 2005) prompted us to evaluate its role in the cardiovascular ECM.

Analysis of adult mice with *Adamts9* haploinsufficiency identified defects specifically involving the outflow tract and myocardium. The data suggest that the pleiotropic effects of *Adamts9* deficiency may have their origin in reduced versican processing during development. This work further suggests a potentially important role for versican cleavage in cardiovascular allostasis, the active process of maintaining the homeostatic state. We propose *ADAMTS9* as a potential candidate gene in congenital valvular, aortic and myocardial anomalies.

2. Results

For these studies, we used an *Adamts9* targeted allele generated by homologous recombination in ES cells. The targeting construct was engineered by insertion of IRES *LacZ-pgk-Neo* in exon 12, encoding contiguous regions of the disintegrin-like module and first thrombospondin type

1 repeat (McCulloch, 2009; Silver et al., 2008). Thus, in these mice, *LacZ* expression is driven by the *Adamts9* promoter, and β-gal staining can be used as a indicator of *Adamts9* mRNA expression (McCulloch, 2009). *In situ* hybridization showed that there was no detectable *Adamts9* RNA in mice homozygous for the *Adamts9 LacZ* insertion ($Adamts9^{LacZ/LacZ}$); therefore these mice are considered null for *Adamts9* expression. Since $Adamts9^{LacZ/LacZ}$, mice die by E7.5, i.e., prior to cardiovascular development (Silver et al., 2008) the effect of complete ADAMTS9 deficiency on cardiac development is presently unknown. However, we identified several phenotypic anomalies in adult hearts of the $Adamts9^{+/LacZ}$ heterozygotes and determined their overall incidence (Phenotypic penetrance, Table 1).

2.1 *Adamts9* expression in the early Secondary Heart Field during outflow tract development is consistent with regions that develop cardiovascular anomalies

Our previous studies using RT-PCR determined that *Adamts9* was expressed throughout cardiac development(Kern et al., 2006) and we further demonstrated mRNA expression in cardiovascular development as part of a study addressing *Adamts9* expression in the developing embryo. Here we have extended this work to determine the precise spatiotemporal expression pattern of *Adamts9* during cardiac development. *Adamts9* expression, defined by X-gal staining (blue) using the $Adamts9^{+/lacZ}$ mouse model was most prominent within the myocardial walls of the outlet at E9.5 (Fig. 1A–D) and E11.5 (Fig. 1E–H). Myocardial cells of the forming cardiac outlet are derived from the SHF and were identified by the transcription factor *islet1* (Fig. 1B, D, F and G). At E11.5 there was strong expression of *Adamts9* (blue) within the right-sided endocardial cushions in the distal part of the OFT (Fig. 1E, asterisk, F box magnified in G) coincident with the loss of the transient myocardial sleeve (Fig. 1E bar, lack of sarcomeric α-actin, brown staining) in contrast to mesenchyme subjacent to the transient myocardium (Fig. 1F, solid arrowheads, brown staining). Myocardium of the SHF is distinguished from the primary myocardium by it's origin and by the fact that it represents the most recently differentiated mesoderm. These myocardial expression data are consistent with the previously published work (Jungers et al., 2005). In each case, *Adamts9* and *Isl1* overlapped in the remodeling truncal cushion (Fig. 1E–H box) and transient myocardial wall. Remodeling of the distal OFT cushions was coincident with α-SMA staining and early formation of arterial tissue (Fig. 1H). Immunolocalization of ADAMTS9 was performed on *Wnt-1 CRE/Rosa26LacZ* sections in which the cardiac neural crest cells were marked by α-gal staining; these studies demonstrated that *Adamts9* is expressed in non-neural crest derived mesenchyme of the semi-lunar valves (Fig. 1I,J, arrow), and SMC of the arterial wall (Fig. 1I, arrowhead). *Adamts9* is also expressed in the valvular sinus (Fig. 1J, VS) derived from the SHF. To localize the cleaved form of versican, the anti-DPEAAE antibody was used. This antibody specifically recognizes the neo-epitope generated upon cleavage of the versican variants V0 and V1 by the ADAMTS proteases and has been used in published studies by our group (Kern et al., 2007; Kern et al., 2006) as well as others (McCulloch, 2009; Sandy, 2001; Silver et al., 2008). The cleaved versican reactive with anti- DPEAAE (Fig. 1K) is found in the leaflets of the aortic and pulmonary arteries, as well as the valvulosinus where *Adamts9* is also expressed. These expression studies demonstrated that *Adamts9* expression was observed throughout cardiac development in multiple cell-types that contribute to remodeling of the cardiovascular ECM. However, retrograde phenotypic analysis of *Adamts9*+/− mice from E9.5–14.5 did not reveal obvious developmental malformations in $Adamts9^{+/lacZ}$ hearts.

2.2 *Adamts9* expression continues in the fibrous extracellular matrix of the adult mouse heart

The expression of *Adamts9* continues in the derivatives of the SHF such as the arterial wall of the aorta, the valvulosinus, as well as regions influenced by the SHF during migration such as the aortic leaflets. X-gal staining was apparent within SMCs of the aortic walls of $Adamts9^{+/LacZ}$ heterozygotes and was consistently more intense in the right side of the wall than on the left side (n=17/17) (Fig. 2A). An example of a malformed right aortic leaflet in the

Adamts9$^{+/LacZ}$ heterozygotes is shown in Fig. 2A (arrow). *Adamts9* expression was also observed in the aortic valves (Fig. 2B) of the adult heart in both the distal leaflet (Fig. 2B, arrow) and the hinge region (Fig. 2B, arrowhead). The β-gal positive cells in the aorta stained with α-SMA (Fig. 2C, green arrowheads); the cells of the aortic adventitia were β-gal positive (Fig. 2C, green arrow), but α-SMA-negative. The hinge region (Fig. 2D, arrowhead) and the valvular interstitial cells of the mitral valve leaflets (Fig. 2D, arrow) are also positive for *Adamts9*. Nonmyocardial cells of the ventricle also express *Adamts9* (Fig. 2E, open arrow). We identified a number of specific anomalies in *Adamts9*$^{+/LacZ}$ mice that are described in detail below and summarized in Table 1.

2.3 Adult *Adamts9*$^{+/LacZ}$ mice developed chondrogenic-like nodules in the valvular sinus region

An example of an *Adamts9*$^{+/LacZ}$ heart with a chondrogenic-like nodule in the valvular sinus region, identified by the typical morphology of chondrocytes and the staining of the surrounding matrix by alcian blue is shown in Fig. 3. Cartilaginous-like nodules were not present in any wild type (WT) mouse hearts examined (n=10), nor have they been reported in the literature as a normal or variable component of the mouse heart. The observation of X-gal stained cells in the nodules (Fig. 2A, box, inset) strongly associates reduced *Adamts9* expression with a local role in the cartilaginous-like nodule, and possibly in its genesis and ongoing growth. Additional examples of *Adamts9*$^{+/LacZ}$ hearts containing cartilaginous-like nodules are shown (Fig. 3A–F). Cell appearances compatible with hypertrophic and non-hypertrophic chondrocytes and alcian blue staining, indicative of proteoglycans aggrecan and versican, were visualized in all these nodules. In addition the lacunae were surrounded by yellow stained ECM indicative of collagen in the movat pentachrome stained sections of these nodules. The phenotypic penetrance of the cartilaginous-like nodules was 29% (n=5/17 *Adamts9*$^{+/LacZ}$ adult hearts).

The cartilaginous-like nodules exhibited strong nuclear staining of phospho(p)-Smad2 staining in the *Adamts9*$^{+/LacZ}$ hearts compared to the valvulosinus region from WT hearts (supplemental Fig.1). While the atrial tissue in both hearts subjacent to the valvulosinus is positive in both the *Adamts9*$^{+/LacZ}$ and WT hearts. While this would suggest that there is altered signaling in these chondrogenic-like nodules, further investigation will be required to determine the mechanisms responsible for generating chondrogenic-like nodules in 29% of the *Adamts9*$^{+/LacZ}$ hearts (Table 1).

2.4 Adult *Adamts9*$^{+/LacZ}$ mice developed abnormal aortic valve leaflets

In contrast to WT mice (Fig. 4A), semi-lunar valves from *Adamts9*$^{+/LacZ}$ hearts had thicker leaflets and were occasionally malformed (Fig. 4B–E). An increase in proteoglycan content in the aortic leaflets of *Adamts9*$^{+/LacZ}$ heterozygotes compared to WT valves was observed in the thickened leaflets (Fig. 4B, C, D, blue staining) using a pentachrome stain, in which alcian blue stains proteoglycan-rich matrix blue. Quantification of the sectional area of aortic valves from *Adamts9*$^{+/LacZ}$ hearts and *Adamts9*$^{+/+}$ (WT) hearts demonstrated that the aortic valve leaflets from *Adamts9*$^{+/LacZ}$ hearts (n=8) were significantly larger than WT (n=6) (P=6.7 × 10^{-7}, Fig. 4F). The increase in cell size appeared to be due to an increase in matrix that corresponded to the blue staining in Movat pentachrome sections; however when cell density of *Adamts9*$^{+/LacZ}$ hearts (n=8) and WT (n=6) hearts was compared, there was no statistically significant difference. These results suggested that either cell proliferation or migration could be affected. However using the cell proliferation marker phosphoHistone H3, we were not able to detect proliferating cells in the aortic leaflets in the adult *Adamts9*$^{+/LacZ}$ hearts, examined to date.

2.5 *Adamts9*$^{+/LacZ}$ mice developed myxomatous mitral valves with versican accumulation

Adamts9$^{+/LacZ}$ mice developed enlarged mitral valves as early as 15 weeks of age (Fig. 5B, C). The mitral valves from *Adamts9*$^{+/LacZ}$ heterozygotes contained increased proteoglycan (Fig. 5B, blue staining), which was identified by immunostaining as versican (Fig. 5D–F, green). Immunololocalization of the α-DPEAAE antibody that detects the ADAMTS N-terminal cleavage fragment of versican was localized to the mitral valves from WT (Fig. 5G) and *Adamts9*$^{+/LacZ}$ hearts (Fig. 5H). Our unpublished studies have localized the ADAMTS versicanase ADAMTS5 to the endocardium of the mitral valves (C. Kern unpublished) consistent with the observed immunoreactivity of DPEAAE in the WT and *Adamts9*$^{+/LacZ}$ valve. Myxomatous degeneration refers to pathological weakening of the organized fibrous components of connective tissue within the mitral valve with accumulation of a highly hydrated matrix enriched in glycosaminoglycans, such as versican, and is also known to occur in the semi-lunar valves. The PH3 marker stained positive in two different examples of abnormal mitral valve phenotype (supplement Fig. 2B, C, F) suggesting that the valvular interstitial cells were proliferating. To date there have not been any reports that normal adult valvular interstitial cells proliferate. Proliferative nodules, were also found on the atrial surface of hearts at 15 weeks of age (supplement Fig. 2E, F) suggesting that myxomatous degeneration in *Adamts9*$^{+/LacZ}$ hearts may be initiated in the endocardium along the atrial surface. The fact that myxomatous valve phenotype was more pronounced in mice greater than 6 months of age suggests that the phenotype is exacerbated with age. Consistent with the possibility of progressive myxomatous change, Adamts9 expression was observed in adult mitral valves (Fig. 2D). Penetrance of myxomatous phenotype is 47% and shown in Table 1.

2.6 *Adamts9*$^{+/LacZ}$ mice developed aortic wall anomalies accompanied by versican accumulation

Aortic wall anomalies were observed in *Adamts9*$^{+/LacZ}$ heterozygotes by 15 weeks of age. After observing a break in the ascending aortic wall in all of the *Adamts9*$^{+/LacZ}$ adult hearts (n=15) after histological processing (Fig. 3A B open arrowhead) and the WT hearts (n=6) had intact arterial walls, was investigated for anomalies of disease. Several different anomalies were observed with variable penetrance summarized in Table 1. The observed abnormalities included an increase in adventitial thickness (n=5/17 *Adamts9*$^{+/LacZ}$ adult heart relative to WT (n=6) hearts concomitant with interruption of the aortic wall (n=17 *Adamts9*$^{+/LacZ}$ adult hearts) (Fig. 6C, white arrow). Morphometric analysis of the 5/17 *Adamts9*$^{+/LacZ}$ adult hearts that displayed adventitial thickness and 4 WT hearts revealed a greater than two fold average adventitial thickness (36.5 μm (+/− 7.37 μm) *Adamts9*$^{+/LacZ}$ to 14.78 μm (+/− 5.03) WT hearts; $P < 3.0 \times 10^{-10}$). In 10/15 *Adamts9*$^{+/LacZ}$ mice disruption and thinning of the aortic elastic lamellae was also observed (Fig. 6D, E, F) in the ascending arterial wall of the aorta. Versican accumulation (detected by anti-GAGβ versican) was also apparent within the aortic and pulmonary walls of *Adamts9*$^{+/LacZ}$ adult hearts (n=2/15) (Fig. 6E, F, H). Accompanying the increased versican staining in the aorta of one of these mice was an extensive cellular infiltrate (Fig. 6F, G), and strong MMP9 staining (Fig. 6H). The infiltrate was observed in every section of the valvulosinus and displayed an increase in versican by both immunolocalization and Movat pentachrome staining. To determine if the increase in cell density in this region was due to an increase in proliferation, PH3 immunolocalization was performed however there was no PH3 detected (data not shown), suggesting that the increase in cell number was due to infiltrating cells. In this region there was substantial thinning of the elastic lamellae. If the increase in cells was due to macrophage Infiltration, rather that SMC proliferation, we hypothesized that MMP9, an elastic degrading MMP would be highly expressed. When MMP9 immunolocalization was performed on the heart with cell infiltrate, there was strong and localized expression of MMP9 within this region (Fig 6H).

Cleaved versican was immunolocalized using the versican ADAMTS cleavage neoepitope antibody anti-DPEAAE in the ascending arterial wall of the aorta (Fig. 7). Quantification of confocal images taken at identical gain settings using Amira™ software showed an average of 4.6 fold less cleaved versican around smooth muscle cells of the tunica media of the ascending aorta of *Adamts9*$^{+/LacZ}$ heterozygotes (n=4) compared to WT (n=4) hearts (Fig. 7).

2.7 *Adamts9*$^{+/LacZ}$ mice have abnormal myocardial projections and interventricular septum

The ventricular myocardium of *Adamts9*$^{+/LacZ}$ hearts displayed abnormal myocardial projections into the left ventricular chamber (Fig. 8B, E, F) compared to WT hearts (Fig. 8A, D). These projections were of irregular size and shape, and were distinct from the papillary muscle projections (Fig. 7B, C, E and F, open arrows). The myocardium from *Adamts9*$^{+/LacZ}$ mice displayed a spongy appearance that was most pronounced near the apex of the heart (Fig. 7H, I). This cross-sectional area of ventricular myocardial tissue compared to space generated upon histological processing between the *Adamts9*$^{+/LacZ}$ hearts and WT hearts was quantified using Amira™ and the data are shown in Figure 7J, ($P = 0.03$). While the spongy myocardial appearance is likely due to change in the ECM and composition between individual cardiomyocytes and between myocardial layers, the cardiomyocytes in the *Adamts9*$^{+/LacZ}$ hearts that are influenced by the surrounding fibroblastic layers were also irregular in appearance and size compared to those in the WT hearts. The cross section width of cardiomyocytes in the outer compact layer as well as in the papillary muscles was measured in WT and heterozygous mice and the data is found in Figure 7K with *Adamts9*$^{+/LacZ}$ hearts and found to be significantly greater ($P = 3 \times 10^{-5}$) in the *Adamts9*$^{+/LacZ}$ hearts compared to WT (n=6). The collective penetrance of myocardial abnormalities including the abnormal projections and the “spongy” appearance in the *Adamts9*$^{+/LacZ}$ hearts is ~90% (**Phenotypic penetrance, Table 1**).

3. Discussion

The expression profile of *Adamts9* during cardiac development and in the adult heart, together with the phenotypic anomalies found in *Adamts9*$^{+/lacZ}$ mice strongly suggest that it is important, and acting locally, in cardiovascular development and/or allostasis. In addition, the data suggest that defects appearing in the presence of *Adamts9* haploinsufficiency could be a consequence of reduced versican proteolysis at these sites. The observed anomalies in the *Adamts9*$^{+/lacZ}$ mice may be due to subtle alterations in remodeling during development or due to a gradual accumulation of uncleaved versican, and/or additional substrates that have not yet been identified, in the adult cardiovascular ECM. The myocardial phenotype is more suggestive of a developmental anomaly of myocardial compaction during late development while the myxomatous mitral valve phenotype exacerbated as the *Adamts9*$^{+/lacZ}$ mice aged, indicating a gradual increase of versican in the adult may contribute to the valvular anomaly or a continued role for ADAMTS9 in sdome capacity other than versican processing. Therefore, we propose that ADAMTS9 is significant for both cardiac development and allostasis.

Although versican proteolysis is associated with remodeling of the versican-rich cushions during development of the OFT (Kern et al., 2007) it has been well established that there is a predominance of the cleaved form of versican in the mature arterial wall (Kenagy et al., 2005; Sandy et al., 2001). Proteoglycans such as versican are distributed within the aorta in a gradient with the greatest concentrations in the intima and adjacent medial layer (Azeloglu et al., 2008). Wight and others have hypothesized that a transmural gradient of proteoglycans plays a significant role in adaptation of the aorta to high shear stress generated by blood flow (Azeloglu et al., 2008). In fact experiments altering blood flow after neointima formation demonstrated that in high blood flow situations, the versican cleavage fragment was increased compared to normal flow conditions. The increase in cleaved versican also correlated with

regression of neointimal thickenings and the loss of proteoglycans (Kenagy et al., 2005). These published data, taken together with the observed anomalies in the mature aorta of the *Adamts9*$^{+/Lacz}$ mice strongly support the concept that the balance of cleaved to intact versican may be important to maintain the integrity of the ECM of the arterial wall as well as to respond to changes in shear stress and injury.

It has been hypothesized that the cleaved fragments of versican can elicit changes in cellular programs different from the intact form (Kern et al., 2007; Longpre et al., 2009; Wight, 2005). Therefore changes in the ratio of intact to cleaved versican due to the heterozygousity of ADAMTS9 may directly signal changes in the SMC phenotype thereby altering the secretion of ECM components or cellular behavior. Conversely, changes in the proteolytic state of versican may indirectly affect a key regulatory network in the vascular wall centered around fibrillin-1, which it binds to through its G3 domain, and consequently, (Isogai et al., 2002; Ohno-Jinno et al., 2008) regulation of TGFβ. In Marfan syndrome, which results from haploinsufficiency of FBN1 (*fibrillin-1*), (Carta et al., 2006; Kielty et al., 2002; Ng et al., 2004; Ramirez et al., 2004), the resulting changes in the arterial ECM have been shown to activate the latent TGFβ complex and result in aortic dissection and rupture (Carta et al., 2006; Judge et al., 2004; Ramirez and Dietz, 2007). Indeed, the consequences of fibrillin-1 deficiency for the aorta do not appear to reflect a purely structural role for fibrillin-1. Rather, they appear to be a consequence of altered TGFβ signaling, since reduction of TGFβ activity mitigates aneurysm progression (Brooke et al., 2008; Habashi et al., 2006). Since versican binds to fibrillin-1 at the C-terminus (Ohno-Jinno et al., 2008), it is possible that the changes in versican proteolysis could affect the role of fibrillin-1 in sequestering latent TGFβ. Although we have found an increase in pSmad2 reactivity in the cartilaginous nodules, further investigation will be required to determine which pathways are involved in initiating cellular signaling changes in response to loss of ADAMTS proteolysis in the cardiovascular ECM.

The reawakening of developmental programs has been shown to be a key component in many cardiovascular diseases including myxomatous mitral valve degeneration, atherosclerosis, and maladaptive myocardial remodeling after a myocardial infarction (Hinton et al., 2006; Latif et al., 2006; Thum et al., 2007). Therefore the known cardiovascular substrate of ADAMTS9, versican, is highly expressed in the intact form during cardiovascular development and therefore an accumulation of versican is also reminiscent of cardiovascular ECM in early development. In fact the increase in proteoglycan content in the *Adamts9* heterozygous mice suggest that the gradual accumulation of intact versican may have reinitiated developmental pathways. In addition, the discovery that *Adamts9*$^{+/lacZ}$ mice develop myxomatous mitral valves offers the possibility that these mice may provide a model of myxomatous degeneration.

While the anomalies of disease in the aorta and the mitral valve of the *Adamts9*$^{+/lacZ}$ may be progress over time, abnormalities observed in the ventricular myocardium of *Adamts9*$^{+/lacZ}$ mice are consistent with developmental myocardial defects observed in previously described mouse models that affect proteoglycan cleavage (Cooley et al., 2008; Stankunas et al., 2008). Abnormal myocardial projections seen in the *Adamts9*$^{+/lacZ}$ mice are suggestive of an alteration of the compaction of trabeculae, which is required to organize the layered myocardial sheaths of the ventricular wall, and papillary muscles in later stages of fetal development. In fact, mice deficient in fibulin-1, which binds to the C-terminus of versican and is a cofactor for ADAMTS1 cleavage of proteoglycans, exhibit hyper-trabeculation consistent with abnormal compaction of the myocardium (Cooley et al., 2008; Lee et al., 2005). Derepression of *Adamts1* also affects trabeculation during development (Stankunas et al., 2008). Myocardial projections in the *Adamts9*$^{+/lacZ}$ mice are comparable with, although milder than the serious clinical disorder, noncompaction of the left ventricle. The widened IVS and spongy myocardium is reminiscent of the Tako-tsubo subtype of the cardiomyopathy, idiopathic hypertrophic subaortic stenosis (IHSS) (Merli et al., 2006). From a clinical perspective,

Adamts9 deficiency clearly results in anomalies involving the myocardium, mitral valves, aortic valves, and proximal aorta therefore we propose *ADAMTS9* as a candidate gene for dominantly inherited or sporadic cases with the full or partial complement of anomalies reported here.

Although the published findings indicate that versican is the only known substrate of ADAMTS9 in the heart, due to the fact that this is a relatively new family of matrix metalloproteases it is highly probable that additional substrates exist in the mouse heart both during development and in the adult that are affected by the loss of ADAMTS9. In addition, due to the complex architecture of the ECM, it may not be the cleavage of versican per se that is responsible for disease but that the reduction in versican cleavage affects the organization of other ECM components that directly contribute to initiation or onset of anomalies of disease in the *Adamts9*$^{+/LacZ}$ adult hearts.

In future studies, it will be essential to develop mouse models that permit conditional deletion of *Adamts9* in the different lineages that constitute the developing heart, as well as to undertake temporally regulated deletion of *Adamts9* to distinguish between its developmental and homeostatic roles. Furthermore, given its overlapping expression with other versican degrading proteases such as *Adamts1* and *Adamts5*, it will be necessary to evaluate mice with combinatorial deletions of *Adamts9* and other versican degrading proteases to uncover the cooperative functions of these proteases in cardiac development.

4. Methods and Materials

4.1 Gene-targeted *Adamts9* LacZ insertion

All mouse experiments were done under a protocol approved by the Cleveland Clinic Foundation's Institutional Animal Care and Use Committee and the Medical University of South Carolina Institutional Animal Care and Use Committee. *Adamts9* heterozygotes were obtained under license from Deltagen (Mouse strain t1235, Palo Alto, CA). Complete details of gene targeting are proprietary and limited information was provided by Deltagen. The targeting construct contained 3.5 kb (5′ end) and 3.0 kb (3′ end) genomic DNA flanking the gene interruption site. 134 nucleotides of exon 12 of the *Adamts9* locus encoding contiguous portions of the disintegrin-like domain and first thrombospondin type-1 repeat were deleted and replaced with an IRES-lacZ-Neomycin resistance cassette. Gene targeting was achieved by homologous recombination following electroporation of mouse 129Ola/Hsd embryonic stem cells and targeted clones were selected using G418 resistance. Correct gene targeting was confirmed by Southern blotting of *Hind* III digests from Neomycin-resistant ES cell clones using a probe outside the 3′ side of the targeting construct and was further validated by PCR using primer pairs specific for the targeted and WT allele. ES cells from a single clone were injected into C57Bl/6 (B6) blastocysts and male chimeras were selected for outbreeding into the B6 strain. Genotyping was done by PCR of tail DNA using a primer common to both WT and targeted alleles (5′CTGATGGTGTTTTGATGCCTCCTC3′) together with either a WT specific primer 5′ATTCACCATAGAGCCAGCACTCAC3′, or a targeted allele-specific primer 5′GACGAGTTCTTCTGAGGGGATCGATC3′. Genotyping of hemizygotes was confirmed by β-galactosidase (β-gal) staining of tail snips, since *Adamts9* is expressed in tails of 1-week old mice. In addition, incorporation of *lacZ* into *Adamts9* was confirmed by extensive β-gal staining of embryos at different gestational stages for comparison with the expression pattern of *Adamts9* previously obtained by *in situ* hybridization (ISH) the profile obtained by β-gal staining was identical to previously reported ISH data (Jungers et al., 2005). *Adamts9*$^{+/LacZ}$ mice were maintained in the B6 strain after extensive backcrossing (>10 generations). *Adamts9*$^{LacZ/LacZ}$ embryos died by E7.5 in both inbred C57BL/6 and hybrid C57BL/6/129Sv strains.

4.2 *Wnt-1 Cre*/R26 Rosa LacZ `marked' Cardiac neural crest lineage

To mark cardiac neural crest cells mating of Wnt-1-Cre (C57Bl/6) provided by Dr. Andrew McMahon, Harvard University, Cambridge, Mass and TgR(ROSA26)26SOR mice were used as described previously (Danielian et al., 1998; Soriano, 1999).

4.3 Antibodies

Rabbit polyclonal antibodies raised against the GAGβ domain of versican were generated by S. Hoffman (Medical University of South Carolina) (Kern et al., 2007). Rabbit polyclonal antibodies against the C-terminal sequence of the neo-epitope of versican V0/V1 generated as a result of proteolytic cleavage (anti-DPEAAE) as initially described by Sandy et al., (2001) and purchased from Affinity BioReagents (Golden, CO). Mouse monoclonal anti-α sarcomeric actin and anti-α-smooth muscle actin were obtained from Sigma Chemical Co., (St. Louis, MO). Rabbit polyclonal antibodies against human MMP-9 were purchased from Abcam (Cambridge, MA). Anti-pSmad2 was purchased from Millipore (Billerica, MA). Goat polyclonal antibodies against ADAMTS9 were purchased from Santa Cruz (Santa Cruz, CA). The hybridoma monoclonal antibody, Islet-1, developed by T. Jessell, was obtained from the Developmental Studies Hybridoma Bank developed under the auspices of the NICHD and maintained by the University of Iowa, Department of Biological Sciences, Iowa City, IA.

4.4 Histology and Immunohistochemistry

Standard histological procedures were used as previously published and inline with printed manufactures protocols. (Kern et al., 2007). For E17.5 Wnt-1Cre-lacZ CNC „marked" sections with overlay immunolocalization (Fig. 1), the transmission mode was used on the Leica SP2 confocal to detect LacZ stained cells. In the same image, emission of the fluorescent conjugated secondary antibodies was detected by sequential scan. In Photoshop™ the image from the transmission mode that shows LacZ stained cells was inverted and placed in the blue channel to overlay detection and to visualize CNC „marked" cells with αSMA, cleaved versican DPEAAE and ADAMTS9. For detection of Islet-1 and p-Smad2 the Vectastain™ Elite ABC Kit (PK-6200, Vector Laboratories, Burlingame, CA, USA) was used to detect primary antibodies.

4.5 Quantification using Amira™ software

To quantify expression from immunohistochemical data, digital images of *Adamts9*$^{+/lacZ}$ and WT heart sections were taken at the same confocal gain settings at the brightest point in the section using the Leica TCS SP2 AOBS Confocal Microscope System (Leica Microsystems Inc., Exton, PA). Using Amira™ software the positive pixels were measured and normalized to total tissue area. Statistical significance was determined using student t-test 2 tailed, type 2 analysis.

Aortic leaflet quantification: To compare aortic leaflet sizes, The total nuclei in the valve leaflets were also counted in two separate sections spanning a depth of at least 40 μm and the number of nuclei/total area was determined in 9 *Adamts9*$^{+/LacZ}$ hearts and 3 WT hearts. Statistical analysis using Student's t-test (2 tailed, type 2) resulted in $P = 0.13$ not significantly different between *Adamts9*$^{+/LacZ}$ hearts and WT hearts.

Myocardial quantification: The spongy appearance of the ventricular myocardium was measured by determining the number of positive pixels in the ventricular muscle and the number of pixels in the separated space between myocardial layers. The number of positive pixels in the separated space is expressed as a percentage over the total number of pixels Error bars represent one standard deviation of the average shown in the bar graph..

Cardiomyocyte size was calculated by measuring the width of myocardial cells cut cross section in the papillary muscle and the ventricular myocardial tissue; a minimum of 75 cardiomyocytes were measured for each area in two hearts each of *Adamts9*$^{+/LacZ}$ and WT. Error bars represent one standard deviation of the average shown in the bar graph.

Supplementary Material

Refer to Web version on PubMed Central for supplementary material.

Acknowledgments

The authors would like to thank Aimee Phelps for her technical expertise in histology that contributed to this work.

Sources of funding: This project was supported by the American Heart Association Beginning Grant in Aid- 076236U (CBK), Grant-in-Aid 0655530U (AW), Grant-in-Aid 0755346U (WSA), Grant-in-Aid 09GRNT2020202 (DRM), and NIH RR0164-34 (CBK, AW, WSA), HL084285 (AW), HL095067 (WSA), HL095696 (DRM), AR49930 (SSA) and AR53890 (SSA).

Non-standard abbreviations and Acronyms

ECM	extracellular matrix
ADAMTS	A Disintegrin-like and Metalloprotease domain with ThromboSpondin type 1 motifs
WT	wild type
OFT	outflow tract
αSMA	smooth muscle alpha-actin.

References

Apte SS. A disintegrin-like and metalloprotease (reprolysin type) with thrombospondin type 1 motifs: the ADAMTS family. Int J Biochem Cell Biol 2004;36:981–5. [PubMed: 15094112]

Apte SS. A disintegrin-like and metalloprotease (reprolysin-type) with thrombospondin type 1 motif (ADAMTS) superfamily-functions and mechanisms. J Biol Chem. 2009

Aspberg A, Adam S, Kostka G, Timpl R, Heinegard D. Fibulin-1 is a ligand for the C-type lectin domains of aggrecan and versican. Journal of Biological Chemistry 1999;274:20444–9. [PubMed: 10400671]

Azeloglu EU, Albro MB, Thimmappa VA, Ateshian GA, Costa KD. Heterogeneous transmural proteoglycan distribution provides a mechanism for regulating residual stresses in the aorta. Am J Physiol Heart Circ Physiol 2008;294:H1197–205. [PubMed: 18156194]

Brooke BS, Habashi JP, Judge DP, Patel N, Loeys B, Dietz HC 3rd. Angiotensin II blockade and aortic-root dilation in Marfan's syndrome. N Engl J Med 2008;358:2787–95. [PubMed: 18579813]

Camenisch TD, Biesterfeldt J, Brehm-Gibson T, Bradley J, McDonald JA. Regulation of cardiac cushion development by hyluronan. Experimental & Clinical Cardiology The Journal of the International Academy of Cardiovascular Sciences 2001;6:4–10.

Camenisch TD, Schroeder JA, Bradley J, Klewer SE, McDonald JA. Heart-valve mesenchyme formation is dependent on hyaluronan-augmented activation of ErbB2-ErbB3 receptors. Nat Med 2002;8:850–5. [PubMed: 12134143]

Capehart AA, Mjaatvedt CH, Hoffman S, Krug EL. Dynamic expression of a native chondroitin sulfate epitope reveals microheterogeneity of extracellular matrix organization in the embryonic chick heart. Anatomical Record 1999;254:181–95. [PubMed: 9972803]

Carta L, Pereira L, Arteaga-Solis E, Lee-Arteaga SY, Lenart B, Starcher B, Merkel CA, Sukoyan M, Kerkis A, Hazeki N, Keene DR, Sakai LY, Ramirez F. Fibrillins 1 and 2 perform partially overlapping functions during aortic development. J Biol Chem 2006;281:8016–23. [PubMed: 16407178]

Cooley MA, Kern CB, Fresco VM, Wessels A, Thompson RP, McQuinn TC, Twal WO, Mjaatvedt CH, Drake CJ, Argraves WS. Fibulin-1 is required for morphogenesis of neural crest-derived structures. Dev Biol 2008;319:336–45. [PubMed: 18538758]

Danielian PS, Muccino D, Rowitch DH, Michael SK, McMahon AP. Modification of gene activity in mouse embryos in utero by a tamoxifen-inducible form of Cre recombinase. Curr Biol 1998;8:1323–6. [PubMed: 9843687]

Dours-Zimmermann MT, Maurer K, Rauch U, Stoffel W, Fassler R, Zimmermann DR. Versican V2 assembles the extracellular matrix surrounding the nodes of ranvier in the CNS. J Neurosci 2009;29:7731–42. [PubMed: 19535585]

Gao G, Westling J, Thompson VP, Howell TD, Gottschall PE, Sandy JD. Activation of the proteolytic activity of ADAMTS4 (aggrecanase-1) by C-terminal truncation. J Biol Chem 2002;277:11034–41. [PubMed: 11796708]

Habashi JP, Judge DP, Holm TM, Cohn RD, Loeys BL, Cooper TK, Myers L, Klein EC, Liu G, Calvi C, Podowski M, Neptune ER, Halushka MK, Bedja D, Gabrielson K, Rifkin DB, Carta L, Ramirez F, Huso DL, Dietz HC. Losartan, an AT1 antagonist, prevents aortic aneurysm in a mouse model of Marfan syndrome. Science 2006;312:117–21. [PubMed: 16601194]

Henderson DJ, Copp AJ. Versican expression is associated with chamber specification, septation, and valvulogenesis in the developing mouse heart. Circulation Research 1998;83:523–32. [PubMed: 9734475]

Hinton RB Jr. Lincoln J, Deutsch GH, Osinska H, Manning PB, Benson DW, Yutzey KE. Extracellular matrix remodeling and organization in developing and diseased aortic valves. Circ Res 2006;98:1431–8. [PubMed: 16645142]

Hutson MR, Kirby ML. Model systems for the study of heart development and disease. Cardiac neural crest and conotruncal malformations. Semin Cell Dev Biol 2007;18:101–10. [PubMed: 17224285]

Isogai Z, Aspberg A, Keene DR, Ono RN, Reinhardt DP, Sakai LY. Versican interacts with fibrillin-1 and links extracellular microfibrils to other connective tissue networks. J Biol Chem 2002;277:4565–72. [PubMed: 11726670]

Ito M, Ishikawa M, Suzuki S, Takamatsu N, Shiba T. A rainbow trout SRY-type gene expressed in pituitary glands. FEBS Lett 1995;377:37–40. [PubMed: 8543013]

Jonsson-Rylander AC, Nilsson T, Fritsche-Danielson R, Hammarstrom A, Behrendt M, Andersson JO, Lindgren K, Andersson AK, Wallbrandt P, Rosengren B, Brodin P, Thelin A, Westin A, Hurt-Camejo E, Lee-Sogaard CH. Role of ADAMTS-1 in atherosclerosis: remodeling of carotid artery, immunohistochemistry, and proteolysis of versican. Arterioscler Thromb Vasc Biol 2005;25:180–5. [PubMed: 15539621]

Judge DP, Biery NJ, Keene DR, Geubtner J, Myers L, Huso DL, Sakai LY, Dietz HC. Evidence for a critical contribution of haploinsufficiency in the complex pathogenesis of Marfan syndrome. J Clin Invest 2004;114:172–81. [PubMed: 15254584]

Jungers KA, Le Goff C, Somerville RP, Apte SS. Adamts9 is widely expressed during mouse embryo development. Gene Expr Patterns 2005;5:609–17. [PubMed: 15939373]

Kelly RG, Brown NA, Buckingham ME. The arterial pole of the mouse heart forms from Fgf10-expressing cells in pharyngeal mesoderm. Dev Cell 2001;1:435–40. [PubMed: 11702954]

Kenagy RD, Fischer JW, Lara S, Sandy JD, Clowes AW, Wight TN. Accumulation and loss of extracellular matrix during shear stress-mediated intimal growth and regression in baboon vascular grafts. J Histochem Cytochem 2005;53:131–40. [PubMed: 15637346]

Kern CB, Norris RA, Thompson RP, Argraves WS, Fairey SE, Reyes L, Hoffman S, Markwald RR, Mjaatvedt CH. Versican proteolysis mediates myocardial regression during outflow tract development. Dev Dyn 2007;236:671–83. [PubMed: 17226818]

Kern CB, Twal WO, Mjaatvedt CH, Fairey SE, Toole BP, Iruela-Arispe ML, Argraves WS. Proteolytic cleavage of versican during cardiac cushion morphogenesis. Dev Dyn 2006;235:2238–47. [PubMed: 16691565]

Kielty CM, Sherratt MJ, Shuttleworth CA. Elastic fibres. J Cell Sci 2002;115:2817–28. [PubMed: 12082143]

Kirby ML, Gale TF, Stewart DE. Neural crest cells contribute to normal aorticopulmonary septation. Science 1983;220:1059–61. [PubMed: 6844926]

Koo BH, Longpre JM, Somerville RP, Alexander JP, Leduc R, Apte SS. Cell-surface processing of pro-ADAMTS9 by furin. J Biol Chem 2006;281:12485–94. [PubMed: 16537537]

Koo BH, Longpre JM, Somerville RP, Alexander JP, Leduc R, Apte SS. Regulation of ADAMTS9 secretion and enzymatic activity by its propeptide. J Biol Chem 2007;282:16146–54. [PubMed: 17403680]

LaPierre DP, Lee DY, Li SZ, Xie YZ, Zhong L, Sheng W, Deng Z, Yang BB. The ability of versican to simultaneously cause apoptotic resistance and sensitivity. Cancer Res 2007;67:4742–50. [PubMed: 17510402]

Latif S, Masino A, Garry DJ. Transcriptional pathways direct cardiac development and regeneration. Trends Cardiovasc Med 2006;16:234–40. [PubMed: 16980180]

Lee NV, Rodriguez-Manzaneque JC, Thai SN, Twal WO, Luque A, Lyons KM, Argraves WS, Iruela-Arispe ML. Fibulin-1 Acts as a Cofactor for the Matrix Metalloprotease ADAMTS-1. J Biol Chem 2005;280:34796–34804. [PubMed: 16061471]

Longpre JM, McCulloch DR, Koo BH, Alexander JP, Apte SS, Leduc R. Characterization of proADAMTS5 processing by proprotein convertases. Int J Biochem Cell Biol 2009;41:1116–26. [PubMed: 18992360]

Margolis R, Margolis R. Aggrecan-versican-neurocan family proteoglycans. Methods Enzymol 1994;245:105–26. [PubMed: 7539091]

McCulloch DR, Dixon LJ, Nelson C, Silver DL, Wylie J, Sasaki T, Cooley MA, Argraves WS, Apte SS. An extracellular network comprising ADAMTS metalloproteases, versican, and fibulin-1 regulates interdigital cell death. Developmental Cell. 2009 In Press.

Merli E, Sutcliffe S, Gori M, Sutherland GG. Tako-Tsubo cardiomyopathy: new insights into the possible underlying pathophysiology. Eur J Echocardiogr 2006;7:53–61. [PubMed: 16182610]

Miyagawa-Tomita S, Waldo K, Tomita H, Kirby ML. Temporospatial study of the migration and distribution of cardiac neural crest in quail-chick chimeras. Am J Anat 1991;192:79–88. [PubMed: 1750383]

Mjaatvedt CH, Nakaoka T, Moreno-Rodriguez R, Norris RA, Kern MJ, Eisenberg CA, Turner D, Markwald RR. The outflow tract of the heart is recruited from a novel heart-forming field. Developmental Biology 2001;238:97–109. [PubMed: 11783996]

Mjaatvedt CH, Yamamura H, Capehart T, Turner D, Markwald RR. The Cspg2 gene, disrupted in the hdf mutant, is required for right cardiac chamber and endocardial cushion formation. Devel. Biology 1998;202:56–66.

Nakamura T, Colbert MC, Robbins J. Neural crest cells retain multipotential characteristics in the developing valves and label the cardiac conduction system. Circ Res 2006;98:1547–54. [PubMed: 16709902]

Ng CM, Cheng A, Myers LA, Martinez-Murillo F, Jie C, Bedja D, Gabrielson KL, Hausladen JM, Mecham RP, Judge DP, Dietz HC. TGF-beta-dependent pathogenesis of mitral valve prolapse in a mouse model of Marfan syndrome. J Clin Invest 2004;114:1586–92. [PubMed: 15546004]

Ohno-Jinno A, Isogai Z, Yoneda M, Kasai K, Miyaishi O, Inoue Y, Kataoka T, Zhao JS, Li H, Takeyama M, Keene DR, Sakai LY, Kimata K, Iwaki M, Zako M. Versican and fibrillin-1 form a major hyaluronan-binding complex in the ciliary body. Invest Ophthalmol Vis Sci 2008;49:2870–7. [PubMed: 18390636]

Perides G, Asher RA, Lark MW, Lane WS, Robinson RA, Bignami A. Glial hyaluronate-binding protein: a product of metalloproteinase digestion of versican? Biochemical Journal 1995;312:377–84. [PubMed: 8526845]

Poelmann RE, Mikawa T, Gittenberger-de Groot AC. Neural crest cells in outflow tract septation of the embryonic chicken heart: differentiation and apoptosis. Developmental Dynamics 1998;212:373–84. [PubMed: 9671941]

Ramirez F, Dietz HC. Marfan syndrome: from molecular pathogenesis to clinical treatment. Curr Opin Genet Dev 2007;17:252–8. [PubMed: 17467262]

Ramirez F, Sakai LY, Dietz HC, Rifkin DB. Fibrillin microfibrils: multipurpose extracellular networks in organismal physiology. Physiol Genomics 2004;19:151–4. [PubMed: 15466717]

Russell DL, Doyle KM, Ochsner SA, Sandy JD, Richards JS. Processing and localization of ADAMTS-1 and proteolytic cleavage of versican during cumulus matrix expansion and ovulation. J Biol Chem 2003;278:42330–9. [PubMed: 12907688]

Sandy JD. Proteoglycan core proteins and catabolic fragments present in tissues and fluids. Methods Mol Biol 2001;171:335–45. [PubMed: 11450246]

Sandy JD, Westling J, Kenagy RD, Iruela-Arispe ML, Verscharen C, Rodriguez-Mazaneque JC, Zimmermann DR, Lemire JM, Fischer JW, Wight TN, Clowes AW. Versican V1 proteolysis in human aorta in vivo occurs at the Glu441-Ala442 bond, a site that is cleaved by recombinant ADAMTS-1 and ADAMTS-4. J Biol Chem 2001;276:13372–8. [PubMed: 11278559]

Sheng W, Wang G, Wang Y, Liang J, Wen J, Zheng PS, Wu Y, Lee V, Slingerland J, Dumont D, Yang BB. The roles of versican V1 and V2 isoforms in cell proliferation and apoptosis. Mol Biol Cell 2005;16:1330–40. [PubMed: 15635104]

Shinomura T, Zako M, Ito K, Ujita M, Kimata K. The gene structure and organization of mouse PG-M, a large chondroitin sulfate proteoglycan. Genomic background for the generation of multiple PG-M transcripts. J Biol Chem 1995;270:10328–33. [PubMed: 7730339]

Silver DL, Hou L, Somerville R, Young ME, Apte SS, Pavan WJ. The secreted metalloprotease ADAMTS20 is required for melanoblast survival. PLoS Genet 2008;4:e1000003. [PubMed: 18454205]

Somerville RP, Longpre JM, Jungers KA, Engle JM, Ross M, Evanko S, Wight TN, Leduc R, Apte SS. Characterization of ADAMTS-9 and ADAMTS-20 as a distinct ADAMTS subfamily related to Caenorhabditis elegans GON-1. J Biol Chem 2003;278:9503–13. [PubMed: 12514189]

Soriano P. Generalized lacZ expression with the ROSA26 Cre reporter strain. Nat Genet 1999;21:70–1. [PubMed: 9916792]

Stankunas K, Hang CT, Tsun ZY, Chen H, Lee NV, Wu JI, Shang C, Bayle JH, Shou W, Iruela-Arispe ML, Chang CP. Endocardial Brg1 represses ADAMTS1 to maintain the microenvironment for myocardial morphogenesis. Dev Cell 2008;14:298–311. [PubMed: 18267097]

Thum T, Galuppo P, Wolf C, Fiedler J, Kneitz S, van Laake LW, Doevendans PA, Mummery CL, Borlak J, Haverich A, Gross C, Engelhardt S, Ertl G, Bauersachs J. MicroRNAs in the human heart: a clue to fetal gene reprogramming in heart failure. Circulation 2007;116:258–67. [PubMed: 17606841]

Verberne ME, Gittenberger-de Groot AC, Poelmann RE. Lineage and development of the parasympathetic nervous system of the embryonic chick heart. Anat Embryol (Berl) 1998;198:171–84. [PubMed: 9764972]

Wight TN. The ADAMTS proteases, extracellular matrix, and vascular disease: waking the sleeping giant (s)! Arterioscler Thromb Vasc Biol 2005;25:12–4. [PubMed: 15626768]

Wight TN. Arterial remodeling in vascular disease: a key role for hyaluronan and versican. Front Biosci 2008;13:4933–7. [PubMed: 18508558]

Wirrig EE, Snarr BS, Chintalapudi MR, O'Neal J L, Phelps AL, Barth JL, Fresco VM, Kern CB, Mjaatvedt CH, Toole BP, Hoffman S, Trusk TC, Argraves WS, Wessels A. Cartilage link protein 1 (Crtl1), an extracellular matrix component playing an important role in heart development. Dev Biol 2007;310:291–303. [PubMed: 17822691]

Wu Y, Chen L, Cao L, Sheng W, Yang BB. Overexpression of the C-terminal PG-M/versican domain impairs growth of tumor cells by intervening in the interaction between epidermal growth factor receptor and beta1-integrin. J Cell Sci 2004;117:2227–37. [PubMed: 15126624]

Wu YJ, La Pierre DP, Wu J, Yee AJ, Yang BB. The interaction of versican with its binding partners. Cell Res 2005;15:483–94. [PubMed: 16045811]

Yang BL, Yang BB, Erwin M, Ang LC, Finkelstein J, Yee AJ. Versican G3 domain enhances cellular adhesion and proliferation of bovine intervertebral disc cells cultured in vitro. Life Sci 2003;73:3399–413. [PubMed: 14572881]

Zako M, Shinomura T, Ujita M, Ito K, Kimata K. Expression of PG-M(V3), an alternatively spliced form of PG-M without a chondroitin sulfate attachment in region in mouse and human tissues. J Biol Chem 1995;270:3914–8. [PubMed: 7876137]

Zanin MK, Bundy J, Ernst H, Wessels A, Conway SJ, Hoffman S. Distinct spatial and temporal distributions of aggrecan and versican in the embryonic chick heart. Anat Rec 1999;256:366–80. [PubMed: 10589023]

Zhang Y, Cao L, Kiani C, Yang BL, Hu W, Yang BB. Promotion of chondrocyte proliferation by versican mediated by G1 domain and EGF-like motifs. J Cell Biochem 1999;73:445–57. [PubMed: 10733339]

Zheng PS, Reis M, Sparling C, Lee DY, La Pierre DP, Wong CK, Deng Z, Kahai S, Wen J, Yang BB. Versican G3 domain promotes blood coagulation through suppressing the activity of tissue factor pathway inhibitor-1. J Biol Chem 2006;281:8175–82. [PubMed: 16431924]

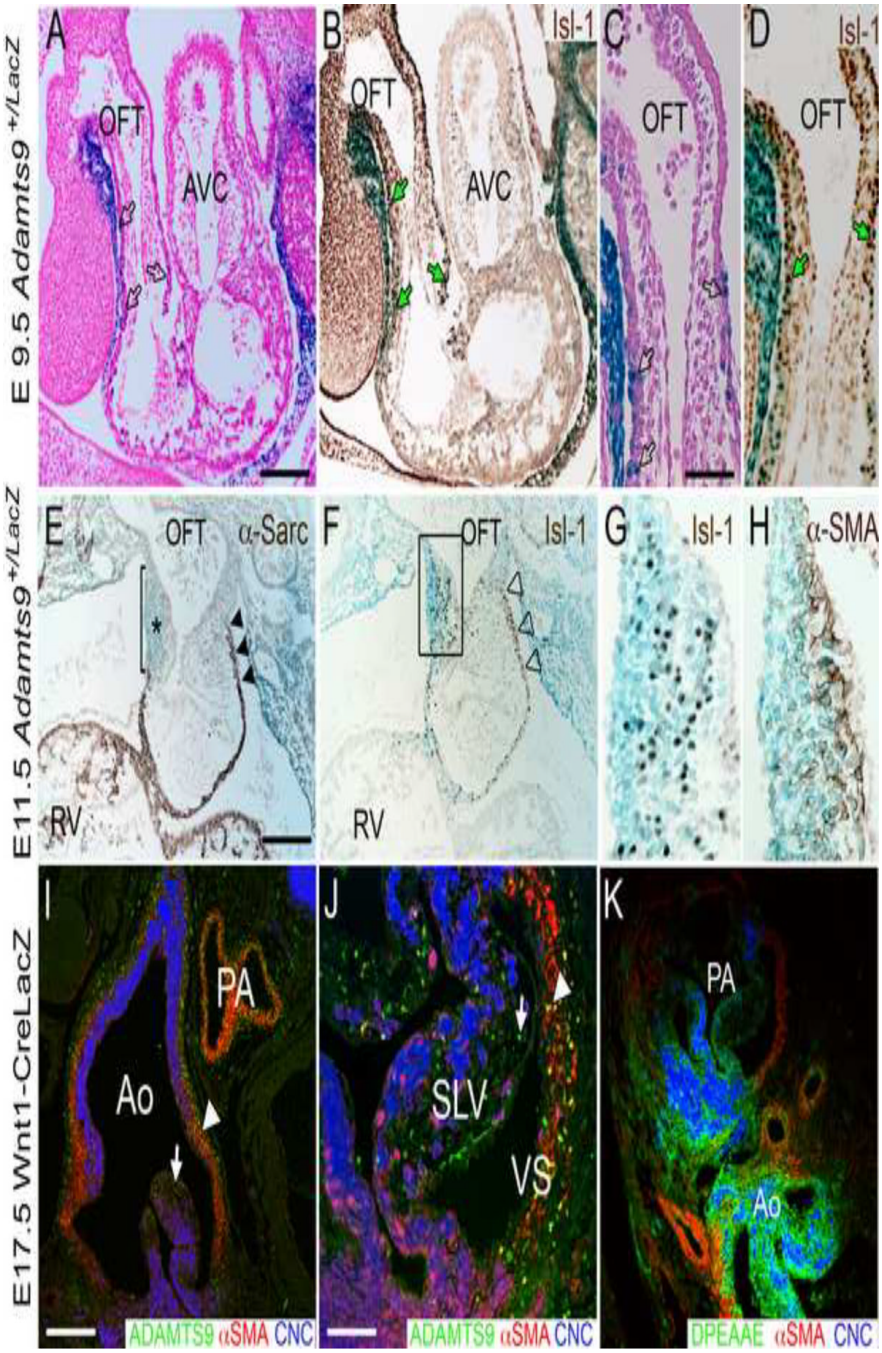

Figure 1. *Adamts9* is expressed at different stages during cardiac development in multiple cell types

Expression of *Adamts9* in the developing cardiac outlet at E9.5 (A–D), E11.5 (E–H) and E17.5 (I,J). A–H show knock-in β-galactosidase (LacZ, blue) expression of *Adamts9*. Panels A and C show *Adamts9* expression present in the transient myocardial sleeve of the OFT at E9.5 (blue, LacZ). *Adamts9* is present in myocardial cells that are Islet-1 (Isl-1) positive (B,D, green arrows) suggesting that they are SHF derivatives. At E11.5 expression of *Adamts9* continues predominantly in the transient myocardial sleeve (blue) (E,F) and in the right truncal cushion (* in E and box in F). α-sarcomeric actin expression is absent subjacent to the right truncal cushion revealing the loss of the transient myocardial wall (bar, E). F shows Isl-1 positive cells in the right truncal cushion, box in F magnified in panel G and shows overlapping *Adamts9*

expression (blue) with *Isl1* (brown). Expression of α-smooth muscle actin is in the subendocardial portion of the truncal cushion and subjacent to the strongest *Adamts9* expression (H). I,J show immunolocalization of ADAMTS9 (green) in the aortic and pulmonary artery walls (arrowhead), as well as in the mesenchymal cells of the semilunar valve leaflets (arrow) at E17.5. K shows a sister section with immunolocalization of the versican neo-epitope DPEAAE (green) cleavage product of versican. OFT-outflow tract; AVC-atrioventricular canal; RV-right ventricle; Ao-aorta; PA-pulmonary artery; SLV-semi-lunar valve; α-sarc- α-sarcomeric actin; α-SMA-α-smooth muscle actin; CNC- cardiac neural crest cells marked with Wnt1-Cre Rosa LacZ in panels I–K; open black arrows (A,C) *Adamts9* expression in the transient myocardial sleeve of the OFT; black arrowheads- *Adamts9* expression in the proximal transient myocardial sleeve; open arrowheads (F) Islet1 in the transient myocardial sleeve; Magnification bars: A= 200μm applies to B, E and F; C = 50μm and applies to D, G, H and J; I=150μm applies to K.

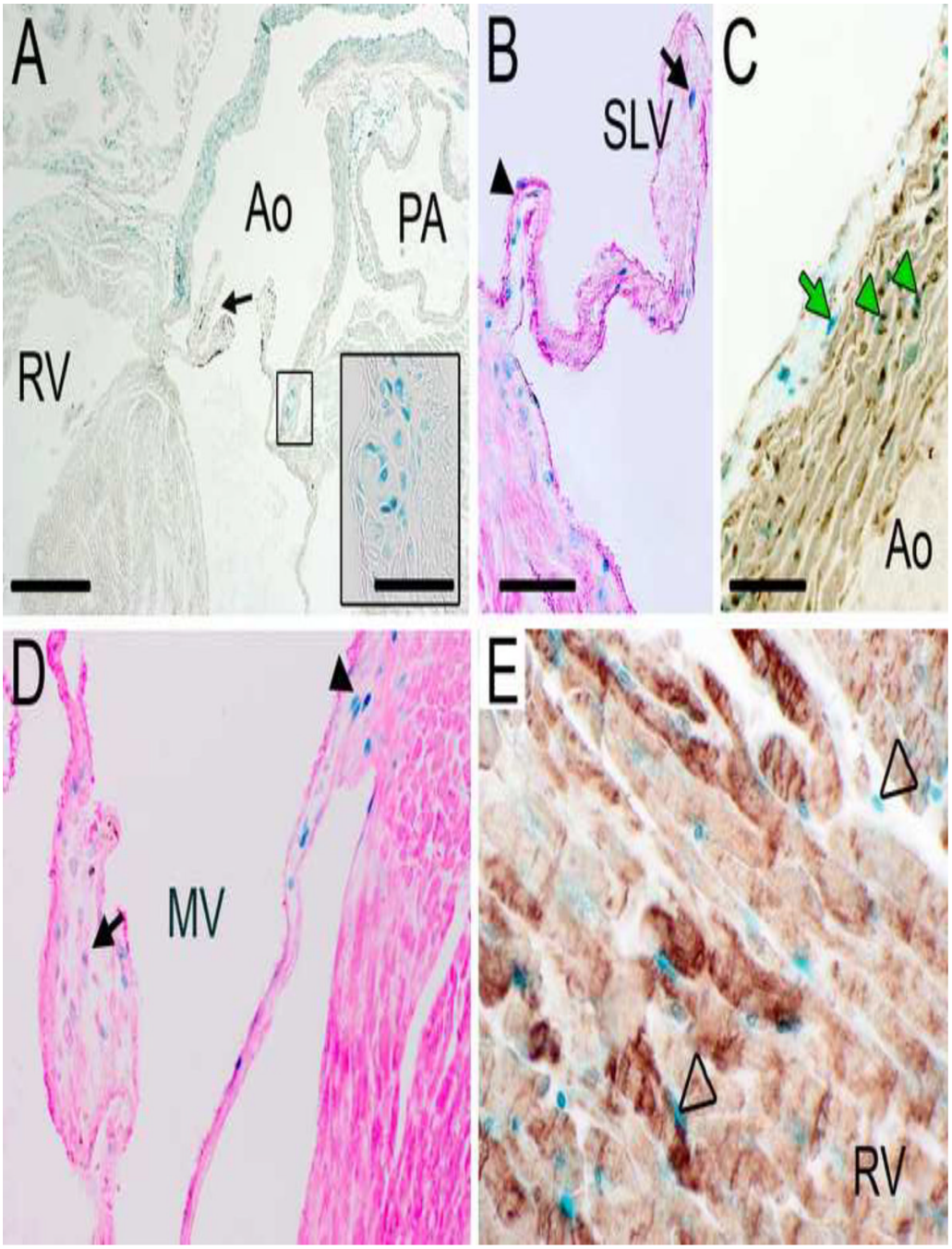

Figure 2. *Adamts9* expression is maintained in connective tissues of the adult heart

Frontal section through an adult *Adamts9*$^{+/LacZ}$ heart reveals *Adamts9* expressing due to β-galactosidase gene expression (LacZ, blue) in the arterial wall of the aorta (Ao). The abnormal presence of a chondrogenic-like nodule in the valvular sinus (A, black box, inset). An abnormal semi-lunar valve leaflet is also shown (A, black arrow). *Adamts9* expression in the hinge region (arrowhead) of the semi-lunar valve and leaflet (arrow) (B). The right ascending aortic arterial wall immunostained with αSMA (C; αSMA, brown). αSMA- alpha smooth muscle actin; Green arrowheads-colocalization of αSMA with *Adamts9*; Green arrow- *Adamts9* expressing cells in the adventitia. *Adamts9* expression in the VIC of the mitral valve leaflet (arrow) and hinge region (arrowhead) (D). Expression of *Adamts9* in noncardiomyocytes within the ventricular

myocardium (E, open arrowheads); cardiomyocytes are identified with anti-alpha sarcomeric actin (E, brown). PA- pulmonary artery; MV- mitral valve. Mag bars: A = 475μm, inset = 8μm; B = 200μm applies to D; C = 30μm applies to E.

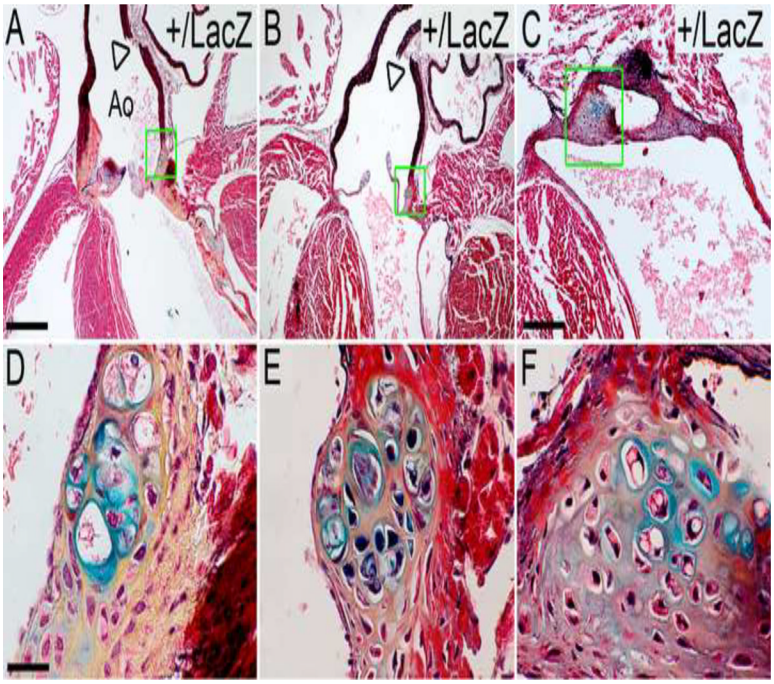

Figure 3. Chondrogenic-like nodules develop in the valvular sinus of *Adamts9*$^{+/LacZ}$ heterozygous hearts

Frontal sections stained with Movat pentachrome of *Adamts9*$^{+/LacZ}$ heterozygous hearts ages 9 (A,D), 15 (B,E) and 24 (C,F) weeks are shown. The areas within the green boxes in A, B, C are shown at higher magnification in D, E, and F respectively. The cells surrounded by blue matrix, indicative of sulfated proteoglycans, are in large lacunae, surrounding the lacunae is collagen (yellow). Boxes in G,H shown magnified in the respective inset. Arrowheads (A, B) denote fractured aortic arterial wall observed in all *Adamts9*$^{+/LacZ}$ heterozygous hearts examined (n=15). Ao-aorta; SLV- semi-lunar valve; At-atrium. Magnification bars: A = 475μm applies to B; C = 200μm; D = 30μm and applies to E and F.

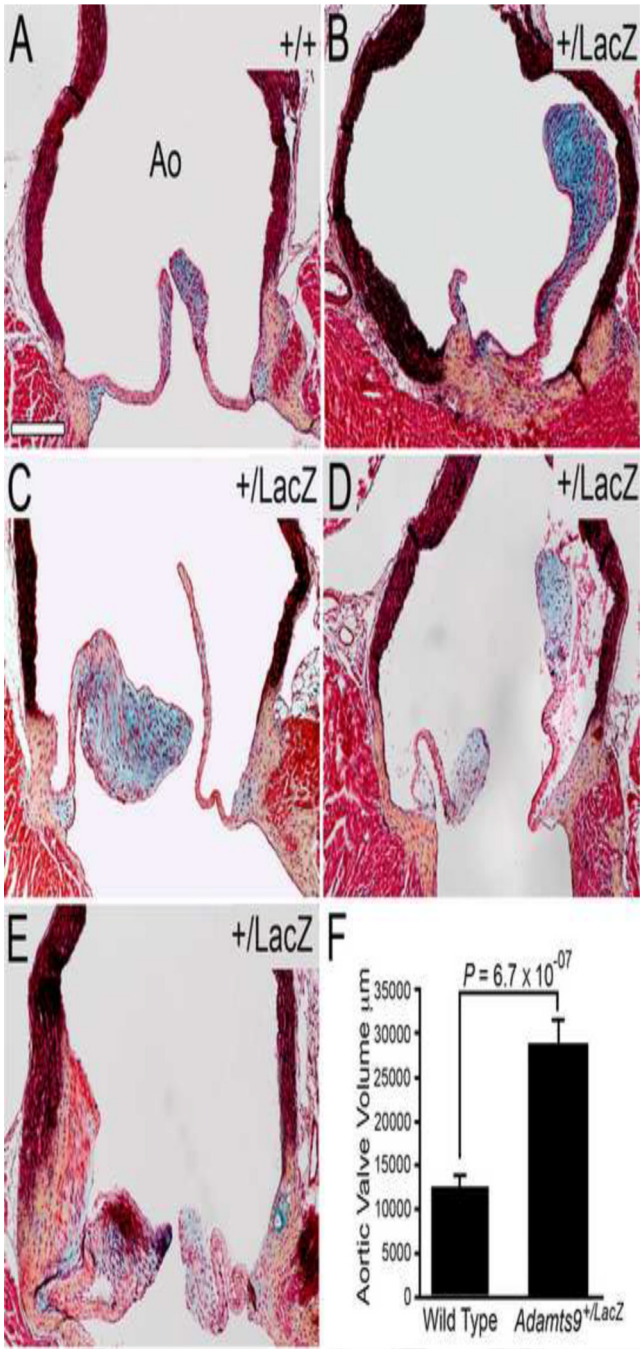

Figure 4. Abnormal aortic valves are seen in *Adamts9*$^{+/LacZ}$ hearts

WT (A) and *Adamts9*$^{+/LacZ}$ heterozygous mouse heart sections (B–E) were stained with the Movat pentachrome stain. Abnormal aortic leaflets (B–E) with an increase in blue staining indicative of an increase in proteoglycans are shown (B, C and D, blue staining overlapped with versican immunoreactivity, data not shown). Quantification of the area of adult WT (n=6) and *Adamts9*$^{+/LacZ}$ heterozygous (n=8) aortic valves is shown in panel F. Area measurements were performed in frontal sections (e.g. Figure 2A and Figure 8A–C) through the widest point of the aorta spanning a minimum of 40 μm width in 9 *Adamts9*$^{+/LacZ}$ hearts and 3 WT hearts. The total area of valves in pixels was compared and the *P* value determined by Student t-test (2 tailed, type 2) was $P = 6.7 \times 10^{-07}$. The penetrance of the aortic valve phenotype was 8/15

at 53%. The *Adamts9*$^{+/LacZ}$ hearts with the aortic valve phenotype were analyzed in this analysis. The Y axis represents the total number of positive pixels of the semilunar valves measured. Magnification bar in A = 200μm applies to B–E.

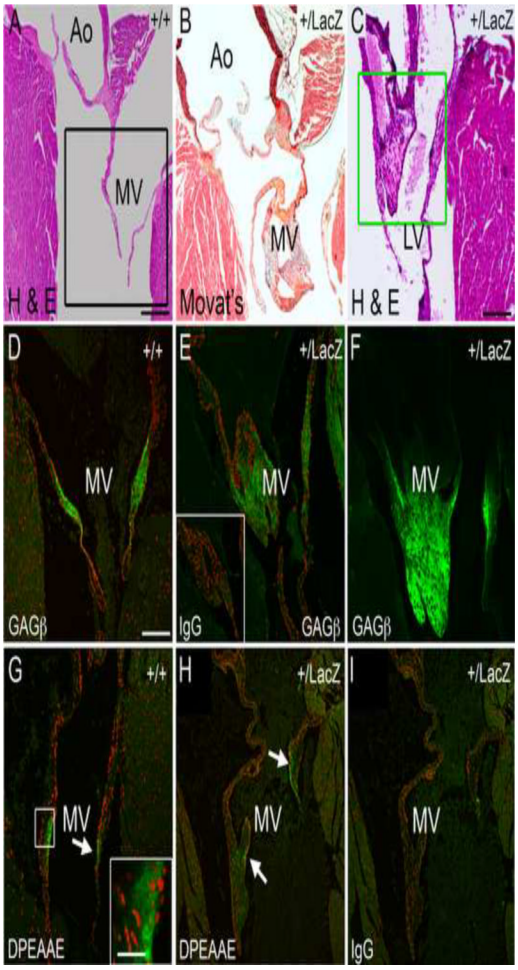

Figure 5. *Adamts9*$^{+/LacZ}$ heterozygous mice develop myxomatous mitral valves

Frontal sections of adult WT (A–C) and *Adamts9*$^{+/LacZ}$ heterozygous hearts (B, C, E, F, H, I) containing abnormal, myxomatous mitral valves. Movat pentachrome stain shows an increase in proteoglycan staining (blue) in an example of an *Adamts9*$^{+/LacZ}$ heterozygous mouse heart (B). Additional examples of *Adamts9*$^{+/LacZ}$ heterozygous hearts with large and irregularly shaped mitral valves (C, E). Sections of WT (D) and *Adamts9*$^{+/LacZ}$ heterozygous hearts (E, F) were immunostained with the αGAGβ antibody for intact versican. IgG antibody control is presented in the inset of E. Black box in A denotes a sister section in D immunostained with αGAGβ antibody. The Green box in F is stained for αGAGβ antibody in F. The N-terminal ADAMTS versican cleavage fragment is localized (G, H) using the αDPEAAE antibody that immunolocalizes the neo-epitope of versican after ADAMTS cleavage (G box and arrow). The box in G is shown in higher magnification in the inset. Magnification bars: A = 475μm applies to B; C = 200μm; D = 150μm and applies to E–I. Inset in G = 10μm.

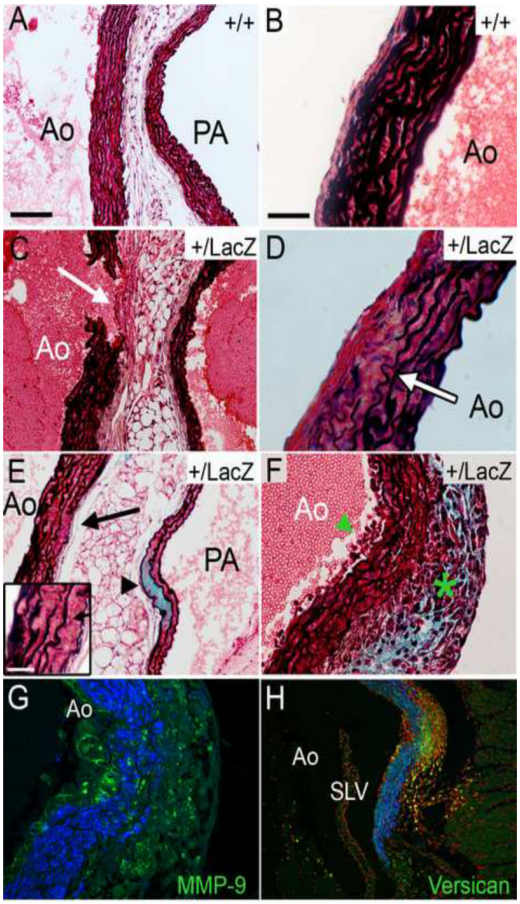

Figure 6. ***Adamts9*$^{+/LacZ}$ heterozygous mice develop anomalies of the aortic wall**

Movat pentachrome-stained sections of the aortic wall. Examples of WT aortic walls (A, left side; B right side). Aortic walls from *Adamts9*$^{+/LacZ}$ heterozygous hearts (C–H). Adventitia thickening (white arrow) adjacent to the aortic break* (C). Irregular and thinning elastic lamellae, containing breaks within the arterial wall from *Adamts9*$^{+/LacZ}$ hearts (D, E-inset, F). *Adamts9*$^{+/LacZ}$ heterozygous aorta shows an increase in the blue staining consistent with an increase in proteoglycans within the pulmonary artery (PA) wall (E, arrowhead). *Adamts9*$^{+/LacZ}$ aortas containing only 6 elastic lamellae (D, E inset), decreased from the normal 8–11 in the ascending aorta (A, B). An *Adamts9*$^{+/LacZ}$ heterozygous heart with an increase in cells associated with the intima (F, green arrowhead) and adventitia (F, green asterisk) with a concomitant increase in proteoglycans (blue). This tunica media shows thinning of elastic lamellae (F). A sister section of panel F was stained with versican (α-GAGβ, green) and αSMA (blue) showing the increase in versican in the region of cell infiltration (G). Sister section of G stained with propidium iodide associated to label cell nuclei immunostained with α-MMP-9 (green) and αSMA (blue) in an *Adamts9*$^{+/LacZ}$ heterozygous heart (H). Magnification bars: A = 100μm applies to C,E,G; Inset E = 8μm; B=30μm and applies to D, F, H). *The thickness of the adventitia was measured in the 5/17 *Adamts9*$^{+/LacZ}$ hearts that displayed the anomaly compared to 4 WT hearts. The average thickness of the *Adamts9*$^{+/LacZ}$ hearts was 36.5 μm (with a standard deviation of the mean +/− 7.37 μm) to 14.78 μm (+/− 5.03) WT hearts with a *P* value 3.0×10^{-10}.

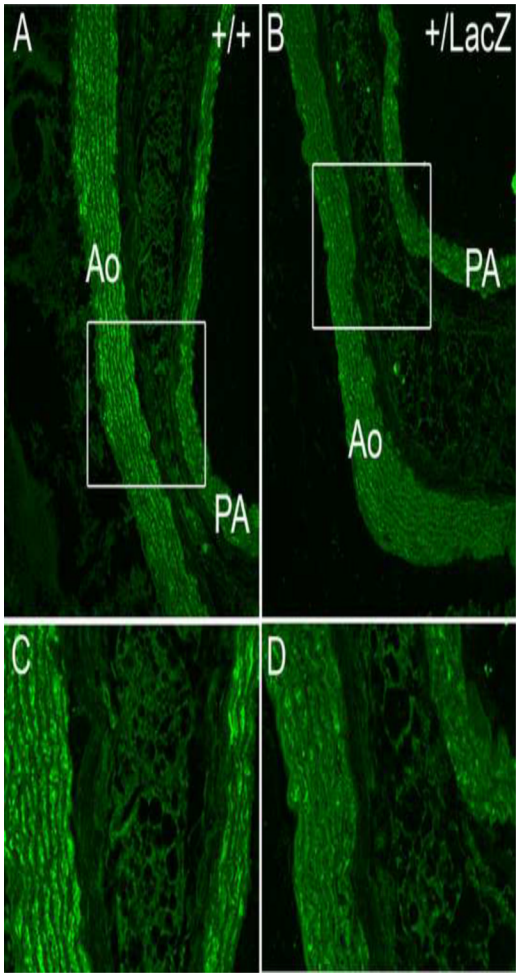

Figure 7. Immunoreactivity of the cleaved form of versican, DPEAAE, is reduced in the aortic wall of *Adamts9*$^{+/LacZ}$ heterozygous mice

WT (A,C) and *Adamts9*$^{+/LacZ}$ heterozygous (B,D) adult aortas immunostained with the DPEAAE antibody detecting the N-terminal cleaved fragment of versican (green). Quantification of expression using Amira™, normalized to area in adult WT (n=4) and *Adamts9*$^{+/LacZ}$ heterozygous (n=4) hearts showed an average of 4.6 fold higher levels of DPEAAE reactivity in WT hearts.

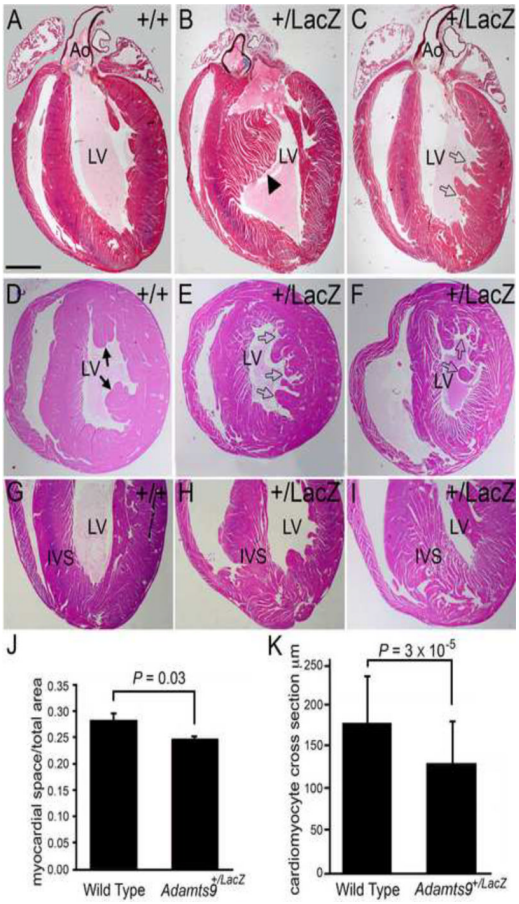

Figure 8. Ventricular myocardium of *Adamts9*$^{+LacZ}$ heterozygous mice have abnormal myocardial projections

WT (A,D,G) and *Adamts9*^{LacZ} heterozygous (B,C,E,F,H,I) adult hearts containing abnormal myocardial projections in the left ventricle (open arrows, solid arrowhead). Frontal sections of adult hearts stained with Movat pentachrome (A–C). Cross sections stained with H&E (D–F). Solid arrowhead in B shows an abnormal interventricular myocardial protrusion. Solid arrows-normal papillary muscles. *Adamts9*^{LacZ} heterozygous (H, I) frontal adult heart sections stained with H&E showing a wide IVS at the apex and `spongy' appearance. Morphometric analysis of the myocardial space versus the myocardial tissue from WT and *Adamts9*^{LacZ} heterozygous hearts $P = 0.03$ (J). A total of 9 *Adamts9*$^{+/LacZ}$ hearts and 3 WT hearts were analyzed, the approximate lower half of the ventricular myocardium toward the apex as shown in G–I. The resulting *P* value using Student's t-test 2 tailed, type 2 was P=0.03. Error bars represent one standard deviation of the average presented in the graph (J). Quantification of the individual size of cross sections from WT and *Adamts9*^{LacZ} heterozygous is also shown; $P = 3 \times 10^{-5}$ (K) using a minimum of 75 *Adamts9*^{LacZ} and WT cardiomyocytes from 4 different animals. Ao-aorta; LV-left ventricle; IVS-interventricular septum. Magnification bars: A = 475µm applies to B–I.

Table 1

Phenotypic Penetrance

Cardiac Anomaly	No. of Hearts with Anomaly/Total *Adamts9* heterozygotes Examined	Penetrance (%)
Condrogenic-like Nodules	**5/17**	**29**
Aortic Valves	**8/15**	**53**
Aortic Wall	**11/15**	**73**
Elastic fiber anomalies	4/15	27
Other anomalies (cell infiltration, versican accumulation, thickened adventitia)	7/15	47
Mitral Valve Anomaly	**8/17**	**47**
Nodules	3/17	18
Myxomatous change	5/17	29
Ventricular myocardial anomalies	**12/14**	**86**